IEEE Access
Multidisciplinary | Rapid Review | Open Access Journal

Received October 19, 2017, accepted November 16, 2017, date of publication November 27, 2017,
date of current version February 14, 2018.

Digital Object Identifier 10.1109/ACCESS.2017.2777883

Visible Light Communication Channel Modeling for Underwater Environments With Blocking and Shadowing

FARSHAD MIRAMIRKHANI, (Student Member, IEEE), AND MURAT UYSAL, (Senior Member, IEEE)
Department of Electrical and Electronics Engineering, Ozyegin University, 34794 Istanbul, Turkey
Corresponding author: Farshad Miramirkhani (farshad.miramirkhani@ozu.edu.tr)

This work was supported by the Turkish Scientific and Research Council under Grant 215E119.

ABSTRACT In this paper, we present a comprehensive channel modeling and characterization study for underwater visible light communications. Our study is based on the advanced ray tracing, which allows for an accurate description of the interaction of rays emitted from the lighting source within an underwater environment. Contrary to existing works, which are mainly limited to simplified underwater scenarios, i.e., empty sea, we take into account the presence of human and man-made objects to investigate the effects of shadowing and blockage. The reflection characteristics of the sea surface and sea bottom as well as the water characteristics, i.e., extinction coefficient and scattering phase function of particles, are precisely considered. As case studies, we consider various underwater scenarios with different transmitter/receiver specifications (i.e., viewing angle, aperture size) and different depths from the sea surface. For each environment, we obtain channel impulse responses and present a characterization study where channel parameters, such as channel DC gain, path loss, and delay spread, are obtained.

INDEX TERMS Underwater visible light communications, channel modeling, ray tracing.

I. INTRODUCTION

There has been an increasing demand for high-speed real-time underwater wireless links to accommodate a wide range of applications such as environmental monitoring and pollution control, underwater exploration, scientific data collection, maritime archaeology, offshore oil field exploration, port security and tactical surveillance among others. Although fiber optic links are currently used in some underwater applications to establish real-time communication, their high installation cost, operational difficulties and lack of flexibility for redeployment become restrictive for most cases. Wireless communication is a promising alternative and an ideal transmission solution for underwater applications.

Underwater wireless transmission can be achieved through radio, acoustic, or optical waves. Radio frequency waves suffer from significant attenuation in water, which seriously limits the transmission range to very short distances with practical antenna sizes. On the other hand, acoustic waves can support transmission ranges on the order of kilometers and become the typical choice in the commercially available underwater modems. Acoustic systems however fall short with their low data rates (kilobits per second) for emerging bandwidth-hungry underwater applications such as image and real-time video transmission.

As diverse and data-heavy underwater applications emerge, there has been an increasing attention on optical transmission [1], [2] as a powerful alternative and/or complementary to acoustic counterparts. Since water is relatively transparent to light in the blue and green bands of the optical spectrum, visible light sources can be particularly used as wireless transmitters. Underwater visible light communication (UVLC) has therefore emerged as a cost-effective, energy-efficient and high-data-rate technology.

Underwater light propagation is fully modelled by the radiative transfer equation (RTE) [3, Ch. 9] which basically describes the energy conservation of a light wave traversing a scattering medium. RTE involves integro-differential equation of time and space which does not yield a general analytical solution [4]. Thus, some approximate analytical solutions have been proposed [5]–[7] which build upon various simplifying assumptions and the predicted irradiances are typically accurate to a few tens of percent at best, and

can be off by an order of magnitude. Alternatively, numerical methods can be used to solve the RTE. One of these methods is the invariant imbedding solution [8] which is restricted to one spatial dimension and to simple boundary conditions. Another method is the discrete ordinates solution that can only be applied to homogeneous water bodies [9].

As a more flexible tool, Monte Carlo simulations are widely used in the literature for channel modelling [10]–[19]. These studies employ statistical methods and determine the channel characteristics by generating numerous photons and then simulating the interactions of each photon with the medium. Gabriel *et al.* [10] utilized Monte Carlo approach and quantified time dispersion for link ranges up to 100 m in pure sea, clear ocean, coastal and harbor water. Tang *et al.* [11] quantified the path loss of non-line-of-sight (NLOS) underwater links taking into account the effects of random sea surface in clear ocean and coastal water, respectively. Guerra *et al.* [12], [13] modeled the seawater surface as a random variable and quantified the received intensity for various ranges. Liu *et al.* [14] quantified the path loss assuming various transmitter divergence angles and receiver field of views in clear ocean, coastal and harbor water. Dong *et al.* [15] considered a multiple-input multiple-output (MIMO) scenario and computed received intensity for coastal and harbor water. They also obtained a closed form expression for channel impulse response (CIR) using weighted double Gamma function. Akhoundi *et al.* [16] considered a cellular underwater wireless network and obtained channel coefficients of both uplink and downlink for link ranges up to 50 m in clear ocean, coastal and harbor water. Jamali *et al.* [17], [18] considered a relay-assisted underwater system and obtained the CIRs in clear ocean and coastal water for both collimated and diffused laser beams. Wang *et al.* [19] proposed a path loss model as a weighted linear function of two exponentials that can be interpreted as a modified version of the Beer-Lambert law. They applied least mean square (LMS) fitting algorithm to the simulated data to obtain the weighting coefficients.

While earlier works in [10]–[19] demonstrate the feasibility of UVLC and quantify the path loss for different water types, they are limited to simplified underwater scenarios, i.e., empty sea. In this paper, we carry out a channel modeling and characterization study taking into account the presence of human and man-made objects to investigate the effects of shadowing and blockage. For this, we use advanced ray tracing which allows an accurate description of the interaction of rays emitted from the lighting source within an underwater environment. The three dimensional simulation environment is created in Zemax® and enables us to specify the geometry of the underwater environment, the objects within, as well as the specifications of the sources, i.e., lasers or light emitting diodes (LEDs), and receivers, i.e., photodiodes. The reflection characteristics of the sea surface and sea bottom as well as the water characteristics, i.e., extinction coefficient and scattering phase function of particles, are further considered. For a given number of rays, the non-sequential ray tracing tool calculates the detected power and path lengths from source to detector for each ray. These are then imported to Matlab® and processed to yield the CIR.

The remainder of the paper is organized as follows. In Section II, we describe the methodology adopted for channel modelling. In Section III, we confirm the accuracy of our approach with comparison to the existing results reported for empty sea. In Section IV, we present CIRs for more realistic underwater environments including divers, underwater vehicles etc and investigate the associated effects of shadowing and blockage. We finally conclude in Section V.

II. METHODOLOGY FOR CHANNEL MODELING

A summary of major steps followed in the adopted channel modeling methodology is provided in Fig. 1. In the first step, we create a three dimensional simulation environment in Zemax® where the geometry of the underwater environment and the objects therein are defined. The CAD objects can be imported in the simulation platform to model the human beings and any other man-made/natural objects, e.g., underwater vehicles, divers, rocks, etc. Wavelength-dependent reflectance of surface coating for each object in the environment is specified. We further take into account the effects of sea surface and bottom. We assume mud for the sea bottom and consider purely diffuse reflections.

To characterize the reflection and refraction of transmitted rays from the sea surface, we use Fresnel equations respectively given by [20]

$$R_s = \left| \frac{n_1 \cos\theta_i - n_2 \cos\theta_t}{n_1 \cos\theta_i + n_2 \cos\theta_t} \right|^2 \quad (1)$$

$$R_p = \left| \frac{n_1 \cos\theta_t - n_2 \cos\theta_i}{n_1 \cos\theta_t + n_2 \cos\theta_i} \right|^2 \quad (2)$$

where R_s and R_p are the reflectances for s- and p-polarized light, n_1 and n_2 are the refractive indices of incident and refracting medium, and θ_i and θ_t are the incident and refracting angles.

In the second step, we integrate the laser or LED-based light source in the simulation platform. Different types of light sources can be used as UVLC transmitters. A collimated laser beam has very low divergence on the order of milliradians. On the other hand, LED is a diffuse source and transmits its energy over a large spherical section. A semi-collimated source would either be a laser that has been purposefully diffused or a LED that is focused. The emission pattern and relative spectral power distribution are defined as inputs to the simulation platform for the selected light source. It is also possible to draw the related information for commercially available LEDs from Radiant Source Model (RSM) database [21]. As a receiving element, we use a rectangular aperture with specified dimensions and field of view (FOV).

In the third step, we define the underwater environment characteristics. The inherent optical properties of water, i.e., absorption, scattering and extinction coefficients are defined based on the Haltrin model [22] and depth profiles

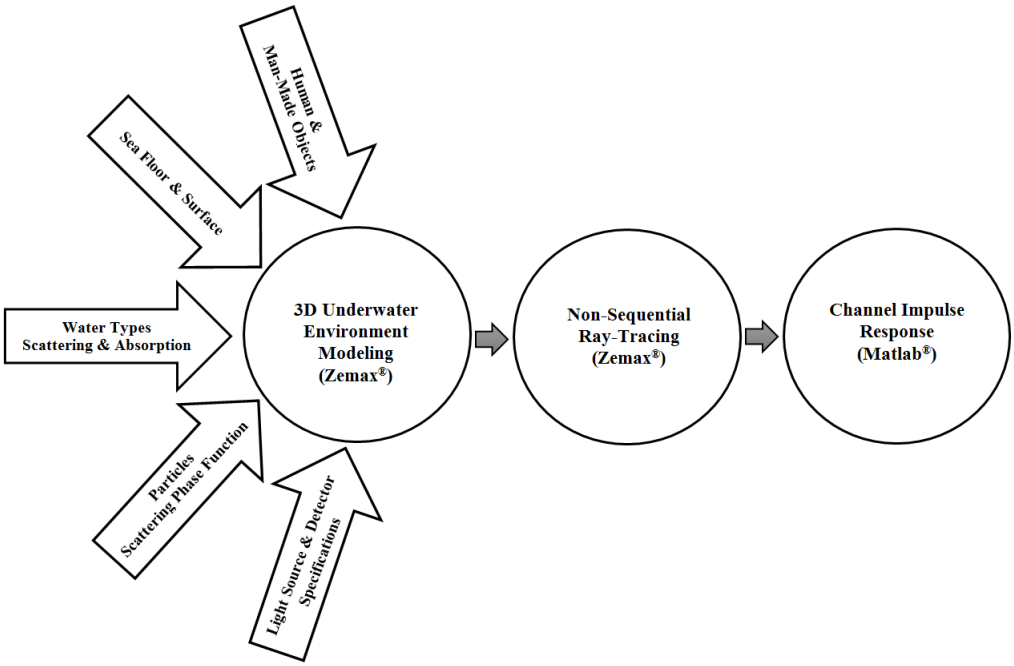

FIGURE 1. Steps in UVLC channel modeling.

of chlorophyll concentration [23]–[25]. In the Haltrin model, the absorption coefficient is expressed as a sum of absorption spectra multiplied by their respective concentrations as

$$a(\lambda) = a_w(\lambda) + a_f^0 \exp(-k_f\lambda)C_f + a_h^0 \exp(-k_h\lambda)C_h + a_c^0(\lambda, z)(C_c/C_c^0)^{0.602} \quad (3)$$

where λ is wavelength and a_w is pure water absorption coefficient (m^{-1}). In the second term of (3), a_f^0 is fulvic acid specific absorption coefficient ($a_f^0 = 35.959$ m^2/mg), k_f is the fulvic acid exponential coefficient ($k_f = 0.0189$ nm^{-1}) and C_f is the concentration of fulvic acid in mg/m^3. In the third term of (3), a_h^0 is the humic acid specific absorption coefficient ($a_h^0 = 18.828$ m^2/mg), k_h is the humic acid exponential coefficient ($k_h = 0.0110$ nm^{-1}) and C_h is the concentration of humic acid in mg/m^3. In the fourth and last term of (3), C_c is the concentration of chlorophyll-a in mg/m^3 (see [25] for calculation of C_c based on depth profiles), $C_c^0 = 1$ mg/m^3 is the reference concentration and a_c^0 is the specific chlorophyll absorption coefficient (m^2/mg) calculated as $a_c^0(\lambda) = A(\lambda)C_c^{-B(\lambda)}$ where coefficients A and B are empirical constants, see [26]. It should be further noted that C_f and C_h are given in terms of concentration of chlorophyll-a as $C_f = 1.74098C_c \exp(0.12327(C_c/C_c^0))$ and $C_h = 0.19334C_c \exp(0.12343(C_c/C_c^0))$ [27].

In the Haltrin model, the scattering coefficient as a function of wavelength and chlorophyll concentration is given by [22]

$$b(\lambda) = b_w(\lambda) + b_s^0(\lambda)C_s + b_l^0(\lambda)C_l \quad (4)$$

where b_w is the pure water scattering coefficient (m^{-1}), b_s^0 is the scattering coefficient for small particulate matter (m^2/g), b_l^0 is the scattering coefficient for large particulate matter (m^2/g), C_s is the concentration of small particles (g/m^3) and C_l is the concentration of large particles (g/m^3). The latter two are given in terms of concentration of chlorophyll-a as $C_s = 0.01739C_c \exp(0.11631(C_c/C_c^0))$ and $C_l = 0.76284C_c \exp(0.03092(C_c/C_c^0))$. The spectral dependencies for the scattering coefficients of small and large particulate matter are given by

$$b_w(\lambda) = 0.005826\big(400/\lambda\big)^{4.322} \quad (5)$$

$$b_s^0(\lambda) = 1.1513\big(400/\lambda\big)^{1.7} \quad (6)$$

$$b_l^0(\lambda) = 0.3411005826\big(400/\lambda\big)^{0.3} \quad (7)$$

The overall attenuation can be then described by the extinction coefficient which can be expressed as the sum of absorption and scattering coefficients, i.e., $c(\lambda) = a(\lambda) + b(\lambda)$.

To model scattering phase function, we use one-term Henyey-Greenstein (OTHG) [28] formula with three parameters, namely mean free path, photon weight updating and average cosine of scattering angle in all scattering directions. The mean free path parameter defines the average geometric distance traveled by photons before being scattered [29] and it can be calculated as the inverse of extinction coefficient ($1/c(\lambda)$). The interaction between the photon and medium may cause the photon losing weight due to the absorption and scattering. The photon therefore needs to update its weight. The photon weight updating is defined as the ratio of scattering coefficient to extinction coefficient, i.e., ($b(\lambda)/c(\lambda)$).

Once the simulation platform is constructed based on the three steps summarized above, non-sequential ray tracing tool

is run to calculate the detected power and path lengths from source to detector for a given number of rays. These are then imported to Matlab® and processed to yield the CIR given by

$$h(t) = \sum_{i=1}^{N_r} P_i \, \delta(t - \tau_i) \tag{8}$$

where P_i is the power of the i^{th} ray, τ_i is the propagation time of the i^{th} ray, $\delta(t)$ is the Dirac delta function and N_r is the number of rays received at the detector. Once we obtain CIRs, we can calculate relevant channel parameters such as channel DC gain, path loss, and root mean square (RMS) delay spread. Channel DC gain is given by [30]

$$H_0 = \int_0^{\infty} h(t)\, dt \tag{9}$$

The path loss can be then expressed as [31]

$$PL = 10 \log_{10} \left(\int_0^{\infty} h(t)\, dt \right) \tag{10}$$

RMS delay spread is commonly used to quantify the time-dispersive properties of multipath channels and is defined as the square root of the second central moment of the CIR, i.e.,

$$\tau_{RMS} = \sqrt{\int_0^{\infty} (t - \tau_0)^2 h(t)\, dt \Big/ \int_0^{\infty} h(t)\, dt} \tag{11}$$

where τ_0 is the mean excess delay spread defined as

$$\tau_0 = \int_0^{\infty} t h(t)\, dt \Big/ \int_0^{\infty} h(t)\, dt \tag{12}$$

III. COMPARISON WITH EXISTING RESULTS FOR EMPTY SEA

In this section, to confirm the accuracy of our approach, we obtain the CIR as well as associated path loss for an empty underwater environment and compare them with the existing analytical expressions in the literature.

A. PATH LOSS EXPRESSIONS

The path loss is a function of both attenuation loss and geometrical loss. For a collimated source such as a laser diode, geometrical loss is negligible; therefore, the path loss only depends on the attenuation loss. On the other hand, the effect of geometrical loss should be taken into account for the diffused and semi-collimated sources, i.e., LEDs and diffused laser diodes.

Attenuation losses can be calculated through well-known Beer-Lambert law [32] or its modified version in [19]. According to Beer-Lambert law, the attenuation loss is given by [32]

$$PL_{\text{BL}} = 10 \log_{10} \left(e^{-c(\lambda) d} \right) \tag{13}$$

where d is the link range between transmitter and receiver and $c(\lambda)$ is extinction coefficient already defined in Section II. Beer-Lambert law builds upon two implicit assumptions.

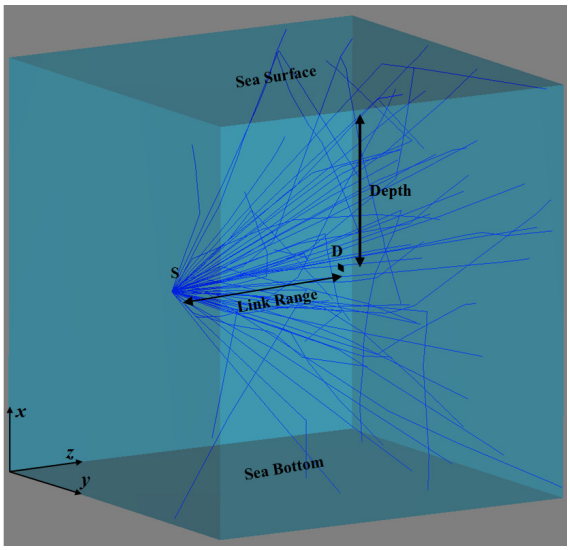

FIGURE 2. Link geometry in empty water environment.

TABLE 1. Simulation parameters.

Transmitter specifications	Power: 1 Watt LED brand: Super Blue Cree® XR-E [33] Viewing angle: 60° [33]
Receiver specifications	Aperture diameter: 5 cm [10] Field of view: 180° [10]
Link range (m)	20
Depth (m)	45
Water type	Coastal-S_8 group (C_c : 0.8 ∼ 2.2 mg/m^3) [25]
Absorption, scattering and extinction coefficients (m^{-1})	0.0508, 0.2116, 0.2624
Scattering phase function	OTHG
Mean cosine of scattering angles (g)	0.9470

First, the transmitter and receiver are perfectly aligned. Second, all the scattered photons are lost even though in reality some of the scattered photons can still arrive at the receiver after multiple scattering events. To address the latter issue, a weighted function of two exponentials is proposed [19] as

$$PL_{\text{MBL}} = 10 \log_{10} \left(u_1 e^{-v_1 d} + u_2 e^{-v_2 d} \right) \tag{14}$$

where the weighting parameters u_1, u_2 , v_1 and v_2 are calculated by the LMS fitting algorithm to the simulation data obtained from Monte Carlo method.

Geometrical loss occurs due to the spreading of the transmitted beam between the transmitter and the receiver. Considering line-of-sight (LOS) configuration and diffused/semi-collimated sources, geometrical loss can be given as

$$PL_{\text{GL}} = 10 \log_{10} \left(\frac{A_R (m+1)}{2\pi d^2} \cos(\phi)^m \right) \tag{15}$$

where A_R denotes the photodetector area, ϕ is the angle of irradiance and $m = -1/\log_2(\cos(\Phi_{1/2}))$ is the order of Lambertian emission where $\Phi_{1/2}$ denotes the semi-angle of the light source. Based on (13-15), the overall path loss can be then determined as the summation of attenuation loss and geometrical loss.

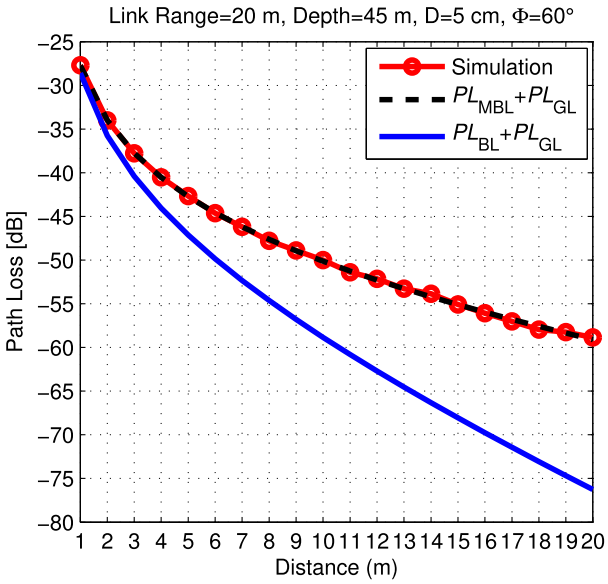

FIGURE 3. Path loss versus distance.

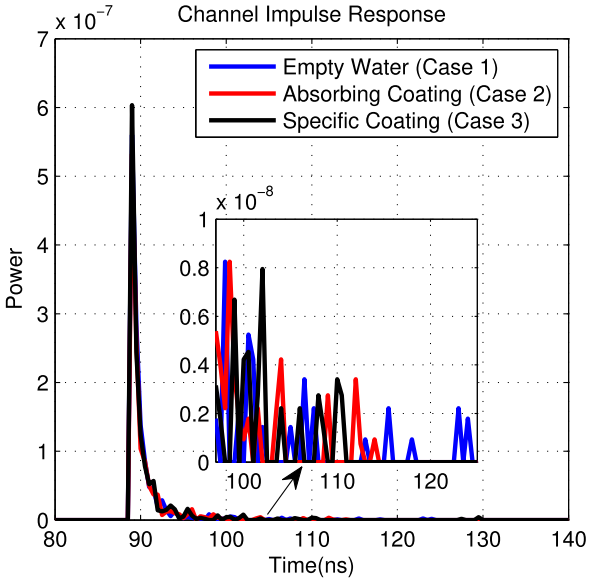

FIGURE 5. Effect of human models on CIR.

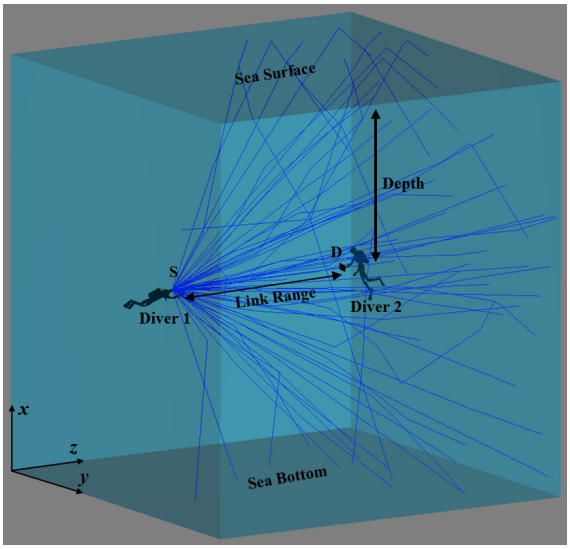

FIGURE 4. Link geometry for two divers who communicate with each other through UVLC link.

B. COMPARISON WITH EXISTING RESULTS

We consider the scenario illustrated in Fig. 2 where the transmitter-receiver pair is placed at a depth of $h = 45$ m with $d = 20$ m distance apart in empty coastal water. The transmitter is selected as a Cree XR-E blue LED with non-ideal Lambertian distribution, a viewing angle of $\Phi = 60°$ and the full width at half maximum spectral of 450-480 nm [33]. The FOV and aperture diameter of the detector are $FOV = 180°$ and $D_R = 5$ cm, respectively. All simulation parameters are summarized in Table 1. CIRs between transmitter and receiver are calculated with 1 meter distance apart.

Path loss is calculated based on (10) and presented in Fig. 3. As benchmarks, we include the path loss expressions calculated through (13-15). The coefficients u_1, u_2 , v_1 and v_2 in (14) are respectively obtained as 1.183, -0.190, 0.072, and 0.164 for the scenario under consideration. It is observed from Fig. 3 that the path loss calculated through our approach is lower than that obtained through Beer-Lambert law. This is expected since Beer-Lambert law is known to overestimate the path loss. On the other hand, our results provide an excellent match with the weighted exponential function of [19].

TABLE 2. Channel parameters for the cases under consideration.

	τ_{RMS} (ns)	H_0	PL (dB)
Case 1	5.27	1.30×10^{-6}	58.85
Case 2	3.22	1.22×10^{-6}	59.11
Case 3	3.89	1.31×10^{-6}	58.79
Case 4	6.28	1.35×10^{-6}	58.68
Case 5	6.77	5.91×10^{-7}	62.27
Case 6	8.22	2.73×10^{-7}	65.63
Case 7	5.71	4.90×10^{-7}	63.09
Case 8	3.44	7.64×10^{-7}	61.16
Case 9	2.26	8.08×10^{-7}	60.92
Case 10	2.17	7.81×10^{-7}	61.07
Case 11	2.14	4.84×10^{-7}	63.14
Case 12	7.88	1.34×10^{-6}	58.72
Case 13	7.08	5.00×10^{-6}	53.00
Case 14	5.42	4.06×10^{-7}	63.90
Case 15	11.25	1.73×10^{-7}	67.60

IV. EFFECTS OF BLOCKING AND SHADOWING

In this section, we present CIRs for more realistic underwater environments including divers, underwater vehicles etc and investigate the associated effects of shadowing and blocking. We assume that there are two divers who communicate with each other through UVLC link (see Fig. 4). The transmitter and receiver are placed in their hands. Unless otherwise stated, we use the simulation parameters provided in Table 1. In the following, we consider several cases to investigate the effect of human modeling, LOS blockage, transmitter/receiver specifications and water depth.

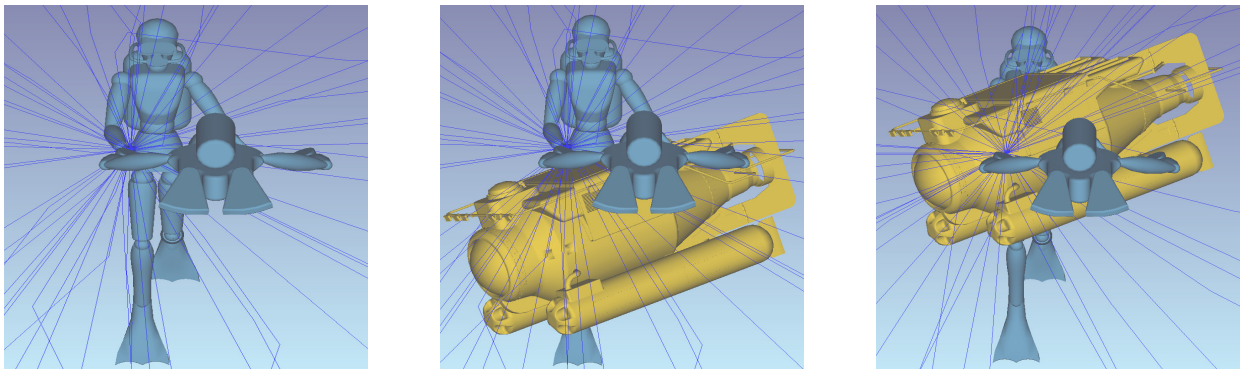

FIGURE 6. (a) Without LOS blockage, (b) partial LOS blockage and (c) complete LOS blockage.

A. PRESENCE OF HUMANS AND EFFECT OF HUMAN MODELING

To demonstrate the effect of human models, we consider a scenario with no blockage. Three cases are investigated as following. As the benchmark, empty water is considered (Case 1) where transmitter and receiver are placed as two floating nodes without the presence of humans in the environment. In Case 2, two divers are considered and modeled as absorbing objects. In Case 3, the coating materials of two divers are explicitly defined. Specifically, the coating materials of diver suit, diver glasses, and oxygen capsule are respectively modeled as black gloss paint, plexiglas and galvanized steel metal. The CIRs obtained for these three cases are illustrated in Fig. 5 while Table 2 lists all the relevant channel parameters. It is observed from Table 2 that the path losses in Cases 2 and 3 are respectively 59.11 dB and 58.79 dB which are more or less the same. Therefore, the simplifying assumption of absorbing material for human models and clothes can be made without losing accuracy. Since the transmitter and receiver are placed in divers hands without any blockage between them, the path loss remains nearly the same as in empty water. On the other hand, the presence of human has some effect on RMS delay spread. In case of empty water, i.e., Case 1, the RMS delay spread is 5.27 ns while this decreases to 3.22 ns and 3.89 ns for Cases 2 and 3, respectively. This is a result of the fact that the rays cannot pass through human bodies and terminated earlier than those rays in empty water.

B. EFFECT OF LOS BLOCKAGE

The objects present in the underwater environment are likely to result in LOS blockage. In this part, to demonstrate this effect, we consider a scenario where two divers communicate with each other while there is an autonomous underwater vehicle (AUV) between them as illustrated in Fig. 6. As a benchmark, a LOS link with no obstructions is considered (Case 4). AUV is assumed to have a galvanized steel metal exterior and, based on its location, it either provides partial LOS blockage (Case 5) or complete LOS blockage (Case 6).

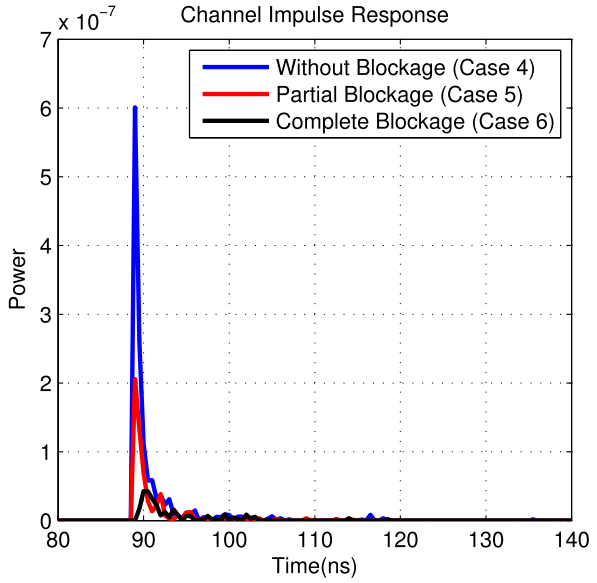

FIGURE 7. Effect of LOS blockage on CIR.

The associated CIRs are provided in Fig. 7. It is observed that the CIR is significantly affected by blockage. In case of complete LOS blockage, the channel DC gain decreases to 20% of the no blockage case (see Table 2). It should be however noted that the receiver still receives some signal due to scattering of light from particles. In terms of path loss, it is observed from Table 2 that the partial LOS blockage introduces an additional loss of 3.59 dB while this climbs to 6.95 dB for complete LOS blockage. Furthermore, as a result of scattered rays from obstructions, additional multipath components are introduced resulting in the increase of RMS delay spread.

C. EFFECT OF TRANSMITTER VIEWING ANGLE

In this part, we investigate the effect of transmitter viewing angles. Complete LOS blockage is assumed. In Fig. 8.a, we illustrate the CIRs assuming $\Phi = 40°$, $20°$, and $10°$ (Case 7, Case 8 and Case 9). In comparison to $\Phi = 60°$ (Case 6 in Fig. 7), it is observed that decrease in LED

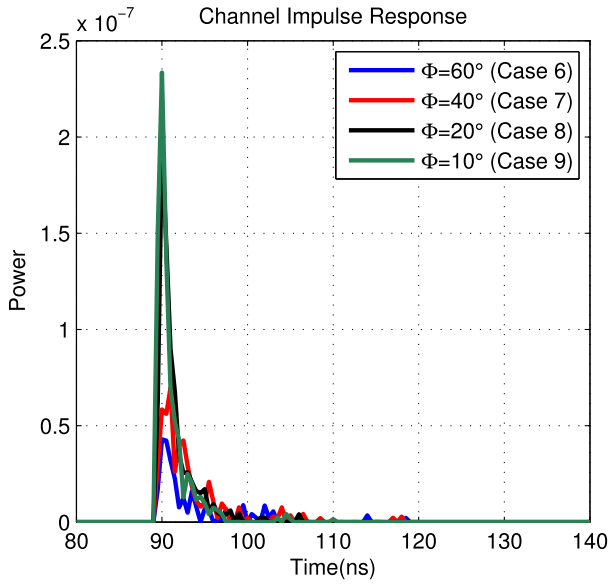

(a)

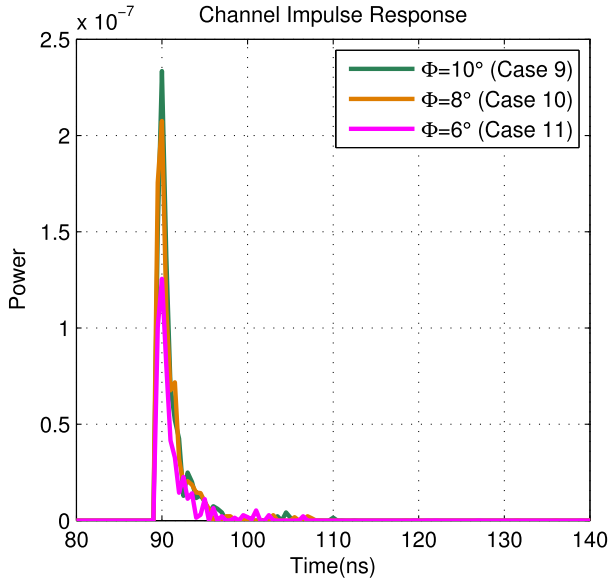

(b)

FIGURE 8. Effect of transmitter viewing angles on CIR.

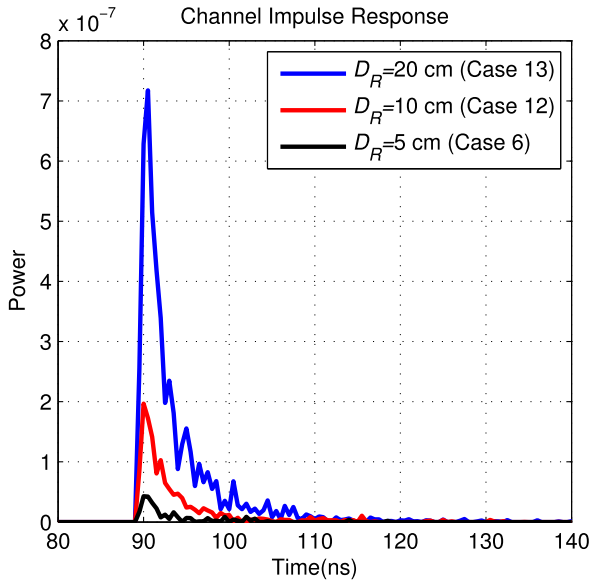

FIGURE 9. Effect of receiver aperture diameters on CIR.

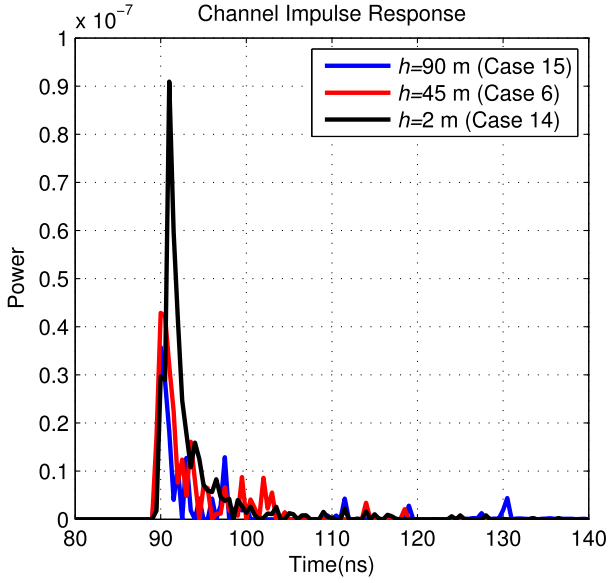

FIGURE 10. Effect of depths on CIR.

viewing angles provide some gains. Specifically, path loss reductions of 2.54 dB, 4.47 dB and 4.71 dB are obtained for $\Phi = 40°$, $20°$, and $10°$, respectively. It is due to the fact that the focused beam has less attenuation through the water medium. It is also observed that RMS delay spread significantly decreases with decreased viewing angles. Specifically, delay spreads of 5.71 ns, 3.44 ns and 2.26 ns are observed for $\Phi = 40°$, $20°$, and $10°$, respectively.

As transmitter viewing angle gets smaller, the improvement in path loss cannot be sustained since the scattered rays are more likely to be blocked by obstruction. To demonstrate this, we illustrate CIRs in Fig. 8.b assuming $\Phi = 8°$ and $6°$ (Case 10 and Case 11). With respect to Case 9 (i.e., $\Phi = 10°$), it is observed that $\Phi = 8°$ results in a loss of 0.15 dB while a loss of 2.22 dB is observed for $\Phi = 6°$. Therefore, $\Phi = 10°$ can be considered as the most appropriate value for the scenario under consideration.

D. EFFECT OF RECEIVER APERTURE SIZE

In this part, we investigate the effect of receiver aperture size. Complete LOS blockage is assumed. In Fig. 9, we illustrate the CIRs for $D_R = 10$ cm and $D_R = 20$ cm (Case 12 and Case 13). In comparison to 5 cm (which was earlier considered as Case 6 in Fig. 7), it is observed that increased aperture diameters provide significant gains. Specifically 6.91 dB and 12.63 dB reductions in path loss are obtained for $D_R = 10$ cm and $D_R = 20$ cm, respectively. It is also observed that RMS delay spread decreases with increased aperture diameters, specifically 0.34 ns and 1.14 ns for $D_R = 10$ cm and $D_R = 20$ cm,

respectively, since the rays are likely to reach earlier to a larger receiver due to less number of scattering.

E. EFFECT OF DEPTH

So far, we assumed a depth of 45 m which can be considered as mid-depth. In Fig. 10, we investigate the effect of depth. Based on the Haltrin model [22] and depth profiles of chlorophyll concentration [25], the absorption, scattering and extinction coefficients at depths of 2 m (Case 14) and 90 m (Case 15) are obtained as (0.1005, 0.3505, 0.4510) and (0.0292, 0.0556, 0.0848), respectively. It is observed that the path loss at sea surface is 63.90 dB indicating a reduction of 1.73 dB over that experienced at mid-depth. This is a result of the fact that the detector receives more specular reflected rays from the sea surface. On the other hand, the path loss at sea bottom is 67.60 dB indicating an additional loss of 1.97 dB over that experienced at mid-depth. This is a result of the fact that the rays are attenuated by diffusely reflecting from sea bottom.

V. CONCLUSIONS

In this paper, we have carried out a detailed underwater optical channel modeling and characterization study taking into account the presence of human and man-made objects such as AUV. The objects present in the underwater environment are likely to result in LOS blockage. Our results have demonstrated that, even in complete LOS blockage, transmission can take place due to scattering despite the increase in path loss. Such losses can be recovered by using smaller transmitter viewing angles or larger aperture sizes. However, there is also some trade-off between performance improvement and viewing angle. As the angle gets smaller, the improvement in path loss cannot be sustained since the scattered rays are also likely to be blocked by obstruction. Our results have also demonstrated that the path loss decreases at sea surface compared to that experienced at mid-depth. This is a result of the fact that the detector receives more specular reflected rays from the sea surface. On the other hand, the path loss at sea bottom increases compared to that experienced at mid-depth since the rays are attenuated by diffusely reflecting from sea bottom.

ACKNOWLEDGEMENT

The statements made herein are solely the responsibility of the authors.

REFERENCES

[1] Z. Zeng, S. Fu, H. Zhang, Y. Dong, and J. Cheng, "A survey of underwater optical wireless communications," *IEEE Commun. Surveys Tuts.*, vol. 19, no. 1, pp. 204–238, 1st Quart., 2017.

[2] H. Kaushal and G. Kaddoum, "Underwater optical wireless communication," *IEEE Access*, vol. 4, pp. 1518–1547, 2016.

[3] S. Arnon, J. Barry, G. Karagiannidis, R. Schober, and M. Uysal, *Advanced Optical Wireless Communication Systems*. Cambridge, U.K.: Cambridge Univ. Press, 2012.

[4] C. Li, K.-H. Park, and M.-S. Alouini, "On the use of a direct radiative transfer equation solver for path loss calculation in underwater optical wireless channels," *IEEE Commun. Lett.*, vol. 4, no. 5, pp. 561–564, Oct. 2015.

[5] S. Jaruwatanadilok, "Underwater wireless optical communication channel modeling and performance evaluation using vector radiative transfer theory," *IEEE J. Sel. Areas Commun.*, vol. 26, no. 9, pp. 1620–1627, Dec. 2008.

[6] B. M. Cochenour, L. J. Mullen, and A. E. Laux, "Characterization of the beam-spread function for underwater wireless optical communications links," *IEEE J. Ocean. Eng.*, vol. 33, no. 4, pp. 513–521, Oct. 2008.

[7] B. M. Cochenour, L. J. Mullen, and A. E. Laux, "Spatial and temporal dispersion in high bandwidth underwater laser communication links," in *Proc. IEEE Military Commun. Conf. (MILCOM)*, Nov. 2008, pp. 1–7.

[8] C. Mobley, "A numerical model for the computation of radiance distributions in natural waters with wind-roughened surfaces," *Limnol. Oceanogr.*, vol. 34, no. 8, pp. 1473–1483, 1989.

[9] R. W. Preisendorfer, "Eigenmatrix representations of radiance distributions in layered natural waters with wind-roughened surfaces," Pacific Marine Environ. Lab., Seattle, WA, USA, NOAA Tech. Memo. ERL PMEL-76 (NTIS PB88-188701), 1988.

[10] C. Gabriel, M.-A. Khalighi, S. Bourennane, P. Leon, and V. Rigaud, "Channel modeling for underwater optical communication," in *Proc. IEEE Global Commun. Conf. (GLOBECOME)*, Dec. 2011, pp. 833–837.

[11] S. Tang, Y. Dong, and X. Zhang, "On path loss of NLOS underwater wireless optical communication links," in *Proc. MTS/IEEE OCEANS (OCEANS)*, Bergen, Norway, Jun. 2013, pp. 1–3.

[12] V. Guerra, C. Quintana, J. Rufo, J. Rabadan, and R. Perez-Jimenez, "Parallelization of a Monte Carlo ray tracing algorithm for channel modelling in underwater wireless optical communications," *Proc. Technol.*, vol. 7, pp. 11–19, Jan. 2013.

[13] V. Guerra, O. El-Asmar, C. Suarez-Rodriguez, R. Perez-Jimenez, and J. M. Luna-Rivera, "Statistical study of the channel parameters in underwater wireless optical links," in *Proc. IEEE Int. Work Conf. Bio-Inspired Intell. (IWOBI)*, Jul. 2014, pp. 124–127.

[14] W. Liu, D. Zou, P. Wang, Z. Xu, and L. Yang, "Wavelength dependent channel characterization for underwater optical wireless communications," in *Proc. IEEE Int. Conf. Signal Process., Commun. Comput. (ICSPCC)*, Aug. 2014, pp. 895–899.

[15] Y. Dong, H. Zhang, and X. Zhang, "On impulse response modeling for underwater wireless optical MIMO links," in *Proc. IEEE/CIC Int. Conf. Commun. China (ICCC)*, Oct. 2014, pp. 151–155.

[16] F. Akhoundi, J. A. Salehi, and A. Tashakori, "Cellular underwater wireless optical CDMA network: Performance analysis and implementation concepts," *IEEE Trans. Commun.*, vol. 63, no. 3, pp. 882–891, Mar. 2015.

[17] M. V. Jamali, F. Akhoundi, and J. A. Salehi, "Performance characterization of relay-assisted wireless optical CDMA networks in turbulent underwater channel," *IEEE Trans. Wireless Commun.*, vol. 15, no. 6, pp. 4104–4116, Jun. 2016.

[18] M. V. Jamali, A. Chizari, and J. A. Salehi, "Performance analysis of multihop underwater wireless optical communication systems," *IEEE Photon. Technol. Lett.*, vol. 29, no. 5, pp. 462–465, Mar. 1, 2017.

[19] C. Wang, H.-Y. Yu, and Y.-J. Zhu, "A long distance underwater visible light communication system with single photon avalanche diode," *IEEE Photon. J.*, vol. 8, no. 5, Oct. 2016, Art. no. 7906311.

[20] S. Arnon and D. Kedar, "Non-line-of-sight underwater optical wireless communication network," *J. Opt. Soc. Amer. A, Opt. Image Sci.*, vol. 26, no. 3, pp. 530–539, 2009.

[21] F. Miramirkhani and M. Uysal, "Channel modeling and characterization for visible light communications," *IEEE Photon. J.*, vol. 7, no. 6, pp. 1–16, Dec. 2015.

[22] V. I. Haltrin, "Chlorophyll-based model of seawater optical properties," *Appl. Opt.*, vol. 38, no. 33, pp. 6826–6832, 1999.

[23] T. Kameda and S. Matsumura, "Chlorophyll biomass off Sanriku, northwestern Pacific, estimated by Ocean Color and Temperature Scanner (OCTS) and a vertical distribution model," *J. Oceanogr.*, vol. 54, no. 5, pp. 509–516, 1998.

[24] J. Uitz, H. Claustre, A. Morel, and S. B. Hooker, "Vertical distribution of phytoplankton communities in open ocean: An assessment based on surface chlorophyll," *J. Geophys. Res., Oceans*, vol. 111, no. C8, pp. 1–23, 2006.

[25] L. J. Johnson, R. J. Green, and M. S. Leeson, "Underwater optical wireless communications: Depth dependent variations in attenuation," *Appl. Opt.*, vol. 52, no. 33, pp. 7867–7873, 2013.

[26] A. Bricaud, M. Babin, A. Morel, and H. Claustre, "Variability in the chlorophyll-specific absorption coefficients of natural phytoplankton: Analysis and parameterization," *J. Geophys. Res., Oceans*, vol. 100, pp. 13321–13332, Jul. 1995.

[27] C. Pontbriand, N. Farr, J. Ware, J. Preisig, and H. Popenoe, "Diffuse high-bandwidth optical communications," in *Proc. IEEE OCEANS*, Sep. 2008, pp. 1–4.
[28] L. C. Henyey and J. L. Greenstein, "Diffuse radiation in the Galaxy," *Astrophys. J.*, vol. 93, pp. 70–83, Jan. 1941.
[29] C. D. Mobley, *Light and Water: Radiative Transfer in Natural Waters*. San Francisco, CA, USA: Academic, Jun. 1994.
[30] M. Uysal, F. Miramirkhani, O. Narmanlioglu, T. Baykas, and E. Panayirci, "IEEE 802.15.7r1 reference channel models for visible light communications," *IEEE Commun. Mag.*, vol. 55, no. 1, pp. 212–217, Jan. 2017.
[31] F. Miramirkhani, O. Narmanlioglu, M. Uysal, and E. Panayirci, "A mobile channel model for VLC and application to adaptive system design," *IEEE Commun. Lett.*, vol. 21, no. 5, pp. 1035–1038, May 2017.
[32] C. D. Mobley *et al.*, "Comparison of numerical models for computing underwater light fields," *Appl. Opt.*, vol. 32, no. 36, pp. 7484–7504, 1993.
[33] B. Tian, F. Zhang, and X. Tan, "Design and development of an LED-based optical communication system for autonomous underwater robots," in *Proc. IEEE/ASME Int. Conf. Adv. Intell. Mechatronics (AIM)*, Jul. 2013, pp. 1558–1563.

FARSHAD MIRAMIRKHANI received the B.Sc. and M.Sc. degrees (Hons.) in electronics and communication engineering from the University of Isfahan, Isfahan, Iran, in 2011 and 2014, respectively. He is currently pursuing the Ph.D. degree with Ozyegin University, Istanbul, Turkey, under the supervision of Prof. M. Uysal. He joined the Communication Theory and Technologies (CT&T) Research Group as a Research Assistant in 2014. The LiFi channels developed by Prof. M. Uysal and Mr. Miramirkhani were selected as the LiFi Reference Channel Models by the IEEE 802.15.7r Task Group during the IEEE's latest meeting held in Bangkok, Thailand, in 2015. His current research interests include optical wireless communications, indoor visible light communications, underwater visible light communications, vehicular visible light communications, and channel modeling. He has served as a reviewer for several prestigious journals and conferences for IEEE and OSA societies.

MURAT UYSAL received the B.Sc. and M.Sc. degrees in electronics and communication engineering from Istanbul Technical University, Istanbul, Turkey, in 1995 and 1998, respectively, and the Ph.D. degree in electrical engineering from Texas A&M University, College Station, TX, USA, in 2001. He is currently a Full Professor and the Chair of the Department of Electrical and Electronics Engineering at Ozyegin University, Istanbul. He also serves as the Founding Director of the Center of Excellence in Optical Wireless Communication Technologies. Prior to joining Ozyegin University, he was a tenured Associate Professor at the University of Waterloo, Waterloo, ON, Canada, where he still holds an adjunct faculty position. He has authored some 300 journal and conference papers in his research topics and received over 8000 citations. His research interests are in the broad areas of communication theory and signal processing with a particular emphasis on the physical layer aspects of wireless communication systems in radio and optical frequency bands.

His distinctions include the Marsland Faculty Fellowship in 2004, the NSERC Discovery Accelerator Supplement Award in 2008, the University of Waterloo Engineering Research Excellence Award in 2010, the Turkish Academy of Sciences Distinguished Young Scientist Award in 2011, and the Ozyegin University Best Researcher Award in 2014 among others. He currently serves on the Editorial Board of the IEEE TRANSACTIONS ON WIRELESS COMMUNICATIONS. In the past, he was an Editor of the IEEE TRANSACTIONS ON COMMUNICATIONS, the IEEE TRANSACTIONS ON VEHICULAR TECHNOLOGY, the IEEE COMMUNICATIONS LETTERS, *Wireless Communications and Mobile Computing* (Wiley) journal, and *Transactions on Emerging Telecommunications Technologies* (Wiley), and a Guest Editor of the IEEE JSAC Special Issues on Optical Wireless Communication (2009 and 2015). He was involved in the organization of several IEEE conferences at various levels. He served as the Chair at the Communication Theory Symposium of the IEEE ICC 2007, the Chair at the Communications and Networking Symposium of the IEEE CCECE 2008, the Chair at the Communication and Information Theory Symposium of IWCMC 2011, the TPC Co-Chair at the IEEE WCNC 2014, and the General Chair at the IEEE IWOW 2015. Over the years, he has served on the technical program committee of over 100 international conferences and workshops in the communications area.